Acta Cryst. (1997). B**53**, 880–884

Neutron Diffraction Study of the Ambient-Pressure, Rutile-Type and the High-Pressure, $CaCl_2$-Type Phases of Ruthenium Dioxide

J. HAINES,[a]* J. M. LÉGER,[a] O. SCHULTE[a] AND S. HULL[b]

[a]*Centre National de la Recherche Scientifique, Laboratoire de Physico-Chimie des Matériaux, 1 Place Aristide Briand, 92190 Meudon, France, and* [b]*ISIS Facility, Rutherford Appleton Laboratory, Chilton, Didcot OX11 OQX, England. E-mail: julian@cnrs-bellevue.fr*

(*Received 23 November 1996; accepted 29 May 1997*)

Abstract

The structures of the ambient-pressure, rutile-type and the high-pressure, $CaCl_2$-type phases of RuO_2 were refined by time-of-flight neutron powder diffraction. Refinement of the data obtained from the ambient-pressure phase ($P4_2/mnm$, $Z = 2$) yielded cell constants $a = 4.49307\ (7)$ and $c = 3.10639\ (7)$ Å and an oxygen positional parameter $x = 0.3056\ (1)$. The principal axes of the displacement ellipsoids of the oxygen ions lie along the directions which correspond to the normal coordinate of the B_{1g} soft mode that drives the transition to the $CaCl_2$-type structure. The $CaCl_2$-type phase ($Pnnm$, $Z = 2$) was refined *in situ* at 5.3 (3) GPa and the following cell constants and oxygen positional parameters were obtained: $a = 4.4865\ (5)$, $b = 4.4347\ (5)$, $c = 3.0934\ (3)$ Å, $x = 0.3101\ (5)$ and $y = 0.3005\ (5)$. In the $CaCl_2$-type phase at 5.3 (3) GPa the RuO_6 octahedra are rotated by 1.1 (2)° with respect to their orientation in the rutile-type phase. There is little change in the internal angles of the octahedron between 0.1 MPa and 5.3 GPa. Compression of the octahedron is anisotropic with a much greater reduction of the Ru—O contacts in the *ab* plane.

1. Introduction

Second-order, tetragonal, rutile-type to orthorhombic, $CaCl_2$-type phase transitions at high pressure have been observed for a series of dioxides: SiO_2 (Tsuchida & Yagi, 1989; Kingma, Cohen, Hemley & Mao, 1995), GeO_2 (Haines *et al.*, 1997), SnO_2 (Haines & Léger, 1997), PbO_2 (Haines, Léger & Schulte, 1996*a*), MnO_2 (Haines, Léger & Hoyau, 1995) and RuO_2 (Haines & Léger, 1993). The transition in silica is of particular interest as it occurs at 50 GPa and thus it may be important in relation to the Earth's mantle. A reduction in symmetry from $P4_2/mnm$ to $Pnnm$ occurs at the transition, which corresponds to the softening of a B_{1g} phonon. The rutile $\rightarrow$ $CaCl_2$ transition plays an important role in the various mechanisms proposed for the transformation from the rutile-type structure to various high-pressure structures (Hyde, Bursill, O'Keeffe & Andersson, 1972; Christy, 1993; Haines & Léger, 1993; Haines & Léger, 1997). *In situ* X-ray diffraction studies of RuO_2 indicated that this second-order transition occurs at 5.0 GPa and that it is followed by a first-order transition to a cubic $Pa\bar{3}$ phase at close to 13 GPa (Haines & Léger, 1993; Haines, Léger & Schulte, 1996*b*). The rutile-type phase has been investigated by single-crystal X-ray diffraction (Hazen & Finger, 1981) up to 2.83 GPa; however, the structure was only refined up to 1.11 GPa. The structure of the ambient, rutile-type phase has not yet been refined using neutron diffraction data and no refinement has been performed for the high-pressure, $CaCl_2$-type phase. Neutron diffraction data should allow a valuable insight into the structural differences between these two phases, as unlike X-ray diffraction the oxide anions contribute significantly to the overall scattered intensity.

2. Experimental

The ambient-pressure, neutron diffraction measurements were performed on the Polaris medium-resolution diffractometer (Hull *et al.*, 1992) at the ISIS spallation source. Powdered RuO_2 (Alfa Products; purity 99.9%) was placed in a 5 mm diameter vanadium sample can and intensities were measured at $2\theta = 145°$ using a bank of ^{3}He ionization counters. The acquisition time was of the order of 30 min. Data were obtained over the time-of-flight range 2000–17 000 μs ($d = 1.6188 \times 10^{-4}$ Å μs^{-1} × time-of-flight).

The high-pressure data were collected on the same diffractometer using the Paris–Edinburgh, high-pressure cell (Besson *et al.*, 1992). Torroidal tungsten carbide anvils and Ti–Zr alloy 'null scattering' gaskets were used. The ruthenium dioxide was loaded with fluorinert as a pressure-transmitting medium and the pressure was estimated based on the equation of state of rutile-type RuO_2 (Hazen & Finger, 1981). The initial volume of the sample–fluorinert mixture was 80 mm^3. The pressure was increased to 5.3 (3) GPa and the collection time at this pressure was 6 h in order to obtain high-quality data from the $CaCl_2$-type phase. Detection was performed using a bank of ZnS scintillation detectors covering the range $82 < 2\theta < 98°$ ($d = 2.2194 \times 10^{-4}$ Å μs^{-1} × time-of-flight). The intensity profile was then corrected by

Table 1. *Experimental details*

	0.1 MPa	5.3 (3) GPa
Crystal data		
Chemical formula	RuO_2	RuO_2
Chemical formula weight	133.07	133.07
Cell setting	Tetragonal	Orthorhombic
Space group	$P4_2/mnm$	*Pnnm*
a (Å)	4.49307 (7)	4.4865 (5)
b (Å)		4.4347 (5)
c (Å)	3.10639 (7)	3.0934 (3)
V (Å^3)	62.711 (3)	61.55 (2)
Z	2	2
Radiation type	Neutron	Neutron
Temperature (K)	298	298
Crystal form	Cylinder	Sphere
Crystal size (mm)	Radius 2.5, height 5	Radius 2.5
Crystal colour	Black	–
Data collection		
Diffractometer	Polaris medium resolution diffractometer	Polaris medium resolution diffractometer
Medium	–	Fluorinert pressure transmitting medium
Special mounting	–	Paris–Edinburgh high-pressure cell
Detection	^{3}He ionization counters	ZnS scintillation detectors
Instrument length (m)	12.8119	12.6041
2θ (°)	145	90
TOF_{min} (μs)	2000	2000
TOF_{max} (μs)	17 000	15 000
Refinement		
Gasket	–	Ti–Zr alloy
R	0.041	0.085
R_{wp}	0.034	0.073
R_{exp}	0.032	0.072
Excluded region (μs)	13 113–13 322	12 000–15 000
No. of parameters used	18	22
χ^2	1.12	1.01
Profile function	Type 2 peak function [Voigtian convolved with double exponential decay and switch features (David, Akporiaye, Ibberson & Wilson, 1988)]	Type 2 peak function [Voigtian convolved with double exponential decay and switch features (David, Akporiaye, Ibberson & Wilson, 1988)]
$(\Delta/\sigma)_{max}$	0.040	0.164
Neutron scattering lengths (m)		
b_{Ru}	0.72100×10^{-12}	0.72100×10^{-12}
b_O	0.58050×10^{-12}	0.58050×10^{-12}
Computer programs		
Structure refinement	*TF12LS* (David, Akporiaye, Ibberson & Wilson, 1988)	*MULTI*, see *TF12LS* (David, Akporiaye, Ibberson & Wilson, 1988)

subtracting the essentially featureless pattern of the empty pressure cell and by removing the wavelength dependence of the incident neutron flux and the effects of attenuation of the incident and scattered beams by the pressure cell components, principally the tungsten carbide anvils (Wilson, Loveday, Nelmes, Klotz & Marshall, 1995). Rietveld refinement of the models was performed using the progam *TF12LS* (David, Akporiaye, Ibberson & Wilson, 1988) for the ambient-pressure data and a multiphase version *MULTI* for the high-pressure data in order to account for the diffraction lines due to the WC anvils. The region above 12 000 μs was excluded for the high-pressure structure refinement due to poor counting statistics resulting from the high attenuation by the anvils for long flight times. In addition to the cell constants, atomic positions and anisotropic thermal parameters, five background parameters, one (high-pressure data) or three (ambient-pressure data) peak-shape parameters and the scale factor were varied. In the multiphase refinement a factor related to the amount of each phase present, along with isotropic displacement parameters and one peak-shape parameter for the tungsten carbide, were also included.

3. Results and discussion

The results from the refinement using neutron diffraction data obtained for rutile-type RuO_2, Fig. 1 and Tables 1 and 2, represent an advance with respect to those

Table 2. *Fractional atomic coordinates, and equivalent isotropic and anisotropic displacement parameters ($Å^2$) at 0.1 MPa*

	x	y	z	U_{eq}	U^{11}	U^{12}	U^{13}	U^{22}	U^{23}	U^{33}
Ru	0.0	0.0	0.0	0.0016 (1)	0.0021 (1)	−0.0004 (2)	0.0	0.0021 (1)	0.0	0.0005 (2)
O	0.3056 (1)	0.3056 (1)	0.0	0.0025 (1)	0.0033 (1)	−0.0014 (2)	0.0	0.0033 (1)	0.0	0.0010 (2)

Table 3. *Selected geometric parameters (Å, °) at 0.1 MPa*

Ru—O	1.9418 (4)	O—O^{i}	2.7765 (5)
Ru—O^{i}	1.9845 (3)	O—O^{iv}	3.10639 (7)
O^{ii}—O^{iii}	2.4705 (6)		
O—Ru—O^{i}	90.0	O^{i}—Ru—O^{ii}	103.01 (1)
O—Ru—O^{v}	90.0	O^{ii}—Ru—O^{iii}	76.99 (3)

Symmetry codes: (i) $\frac{1}{2}-x, y-\frac{1}{2}, -\frac{1}{2}-z$; (ii) $\frac{1}{2}-x, y-\frac{1}{2}, \frac{1}{2}-z$; (iii) $x-\frac{1}{2}, \frac{1}{2}-y, \frac{1}{2}-z$; (iv) $x, y, 1+z$; (v) $x-\frac{1}{2}, \frac{1}{2}-y, -\frac{1}{2}-z$.

obtained from X-ray diffraction studies.† In particular, the only free atomic coordinate x(O) was found to be 0.3056 (1) as opposed to 0.3058 (4) (Hazen & Finger, 1981) and 0.3058 (16) (Boman, 1970). It can be seen that neutron diffraction provides for a significant reduction in the standard uncertainty of x(O). In addition, the anisotropic displacement parameters of Ru and O are refined for the first time. The shape of the oxygen displacement ellipsoids are of particular interest as they are elongated along directions perpendicular to the (110) planes, Fig. 2. These directions correspond to the normal coordinate of the B_{1g} soft mode, which drives the second-order phase transition. This is similar to that observed for other rutile-type compounds, which transform to the $CaCl_2$-type structure at high-pressure, *e.g.* SiO_2 (Hill, Newton & Gibbs, 1983), GeO_2, SnO_2 (Baur & Khan, 1971), PbO_2 (D'Antonio & Santoro, 1980; Hill, 1982), MnO_2 (Bolzan, Fong, Kennedy & Howard, 1993) and NiF_2 (Jauch, Palmer & Schultz, 1993).

At high pressure, as in the X-ray diffraction study (Haines & Léger, 1993), the *hkl* reflections for which $h \neq k$ were found to split, indicating an orthorhombic distortion of the parent rutile phase. The neutron diffraction data obtained at 5.3 (3) GPa, Fig. 3, were used to refine a $CaCl_2$ structural model yielding the structural parameters listed in Tables 1 and 4. The

† The numbered intensity of each measured point on the profile has been deposited with the IUCr (Reference: BR0060). Copies may be obtained through The Managing Editor, International Union of Crystallography, 5 Abbey Square, Chester CH1 2HU, England.

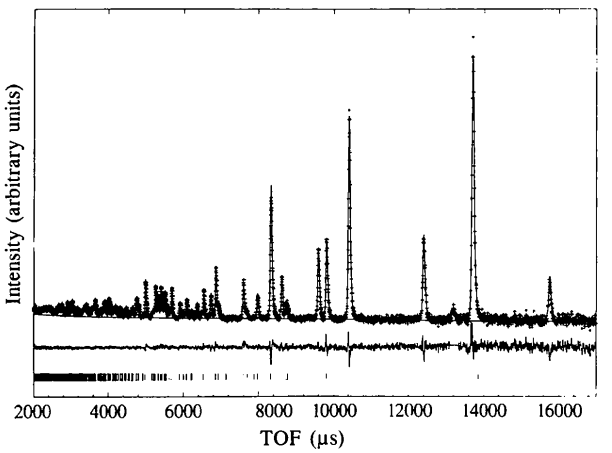

Fig. 1. Experimental (+) and calculated (solid line) profiles from Rietveld refinement of rutile-type RuO_2 at ambient pressure using neutron diffraction data. Intensity is in arbitrary units and the difference profile is on the same scale. Vertical bars indicate the calculated positions of the diffraction lines. The region containing the impurity line at 13 203 μs, which corresponds to the 110 reflection of the vanadium sample can, was excluded from the fit.

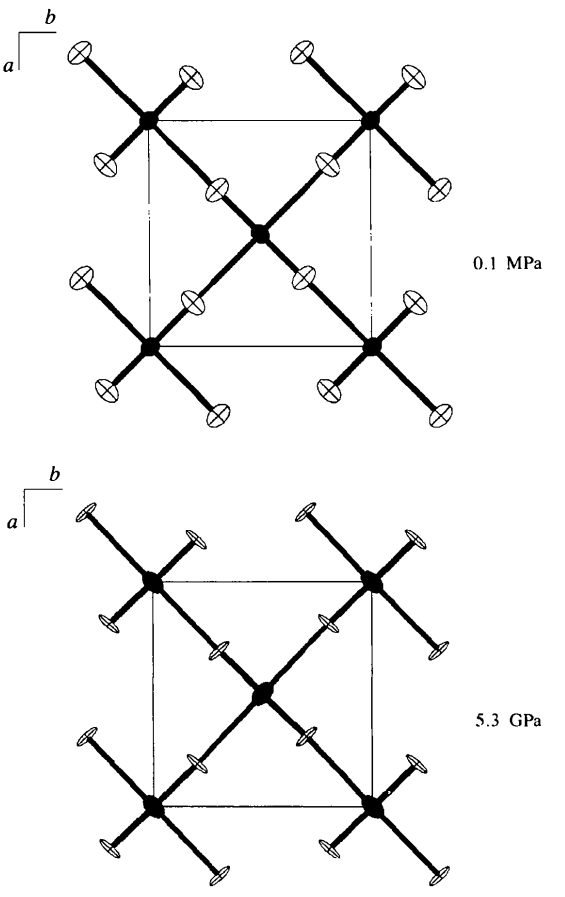

Fig. 2. Projections of the crystal structures of rutile-type RuO_2 at 0.1 MPa (above) and $CaCl_2$-type RuO_2 at 5.3 (3) GPa (below). Atomic displacement ellipsoids are plotted at 99.9% probability. The cations and anions are shaded black and white, respectively.

Table 4. *Fractional atomic coordinates, and equivalent isotropic and anisotropic displacement parameters ($Å^2$) at 5.3 (3) GPa*

	x	y	z	U_{eq}	U^{11}	U^{12}	U^{13}	U^{22}	U^{23}	U^{33}
Ru	0.0	0.0	0.0	0.0022 (3)	0.0030 (8)	0.0013 (5)	0.0	0.0028 (8)	0.0	0.0007 (5)
O	0.3101 (5)	0.3005 (5)	0.0	0.0019 (3)	0.0021 (7)	−0.0020 (4)	0.0	0.0026 (7)	0.0	0.0010 (4)

orthorhombic spontaneous strain $e_{ss} = (a - b)/(a + b) =$ 0.0058 (1) is of the same order of magnitude as that obtained for $CaCl_2$-structured, mixed-metal oxides $Rh_xRu_{1-x}O_2$ and $Cr_xRu_{1-x}O_2$ prepared at pressures of 5–6 GPa and temperatures of 1273–1423 K (Gonzalez-Calbet & Herrero, 1983). It can be noted that the atomic displacements of the oxygen ions are reduced relative to those in the rutile-type phase, whereas a slight increase is observed for the ruthenium displacements.

Both the rutile and $CaCl_2$ structures are composed of chains of edge-sharing RuO_6 octahedra parallel to z, which are crosslinked along the [110] and [1$\bar{1}$0] directions. The atomic displacement resulting from the softening of the B_{1g} mode at the rutile → $CaCl_2$ transition corresponds to the rotation of these chains of octahedra about their twofold axes parallel to z. This rotation of the octahedra relative to the rutile-type structure can be decribed in terms of two angles, ω and ω' (Bärninghausen, Bossert & Anselment, 1984), where

$$\tan(45° + \omega) = b(1/2 - y)/a(1/2 - x) \text{ and}$$
$$\tan(45° - \omega') = by/ax.$$

The angles ω and ω' are 1.1 (2) and 1.2 (1)°, respectively, at 5.3 GPa. These rotation angles are of similar order of magnitude to those observed for the $CaCl_2$-type phase of NiF_2 above the transition at 1.83 GPa (Jorgensen, Worlton & Jamieson, 1978).

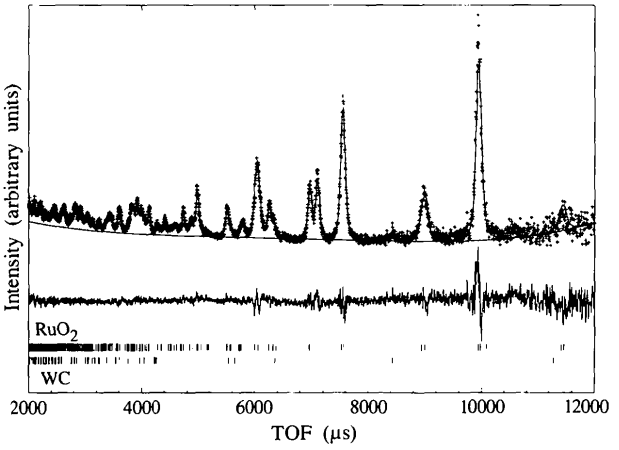

Fig. 3. Experimental (+) and calculated (solid line) profiles from Rietveld refinement of $CaCl_2$-type RuO_2 at 5.3 (3) GPa using neutron diffraction data. Intensity is in arbitrary units and the difference profile is on the same scale. Vertical bars indicate the calculated positions of diffraction lines from $CaCl_2$-type RuO_2 and WC from the anvils of the high-pressure cell.

Table 5. *Selected geometric parameters (Å, °) at 5.5 (3) GPa*

Ru—O	1.926 (2)	O—O^{i}	2.757 (3)
Ru—O^{i}	1.976 (1)	O—O^{iv}	3.0934 (3)
O^{ii}—O^{iii}	2.458 (3)		
O—Ru—O^{i}	89.93 (13)	O^{i}—Ru—O^{ii}	103.06 (6)
O—Ru—O^{v}	90.07 (14)	O^{ii}—Ru—O^{iii}	76.94 (13)

Symmetry codes: (i) $\frac{1}{2} - x, y - \frac{1}{2}, z - \frac{1}{2}$; (ii) $\frac{1}{2} - x, y - \frac{1}{2}, \frac{1}{2} + z$; (iii) $x - \frac{1}{2}, \frac{1}{2} - y, \frac{1}{2} + z$; (iv) $x, y, 1 + z$; (v) $x - \frac{1}{2}, \frac{1}{2} - y, z - \frac{1}{2}$.

It can be noted, Tables 3 and 5, that there is very little change in the internal angles of the octahedra between 0.1 MPa in the rutile-type structure and 5.3 GPa in the $CaCl_2$-type structure and thus the overall angle variance remains essentially constant. The compression of the octahedron is highly anisotropic with the two shorter axial Ru—O contacts undergoing twice the decrease observed for the four longer equatorial Ru—O contacts. The longer contacts bridge the cations along the chain direction, c, whereas the shorter contacts lie in the xy plane and participate in cross-linkages between the chains of edge-sharing octahedra. It can be noted that as a consequence the compressibility in the xy plane is essentially twice that along c between 0.1 MPa and 5.3 GPa. The cation–cation repulsive interactions are much stronger along c due to the short Ru—Ru distance of 3.1064 (1) Å at ambient pressure along this direction. The next shortest Ru—Ru distance, which lies along the [111] direction, is 3.5364 (1) Å. The compressional anisotropy of the octahedra, and as a consequence the unit-cell, is characteristic of rutile-type structures and has been observed for TiO_2 (Kudoh & Takeda, 1986), SiO_2 (Ross, Shu, Hazen & Gasparik, 1990), GeO_2 (Hazen & Finger, 1981), SnO_2 (Haines & Léger, 1997), MnF_2 (Hazen & Finger, 1981) and NiF_2 (Jorgensen, Worlton & Jamieson, 1978).

4. Conclusions

The crystal structures of the rutile-type and $CaCl_2$-type phases of RuO_2 have been refined from neutron diffraction data. The principal changes between 0.1 MPa in the rutile-type structure and 5.3 (3) GPa in the $CaCl_2$-type structure are a rotation of the RuO_6 octahedra by 1.1 (2)° and a reduction in the octahedral Ru—O distances; however, there is no significant increase in the angle variance of the octahedra. The compression of the octahedron is anisotropic due to the

effect of cation–cation repulsion and bridging Ru—O bonds along the chain direction.

Neutron diffraction experiments were performed at the Rutherford Appleton Laboratory under the EC 'Human Capital and Mobility – Access to Large Scale Facilities' programme.

References

Bärninghausen, H., Bossert, W. & Anselment, B. (1984). *Acta Cryst.* A**40**, C-96.

Baur, W. H. & Khan, A. A. (1971). *Acta Cryst.* B**27**, 2133–2139.

Besson, J. M., Nelmes, R. J., Hamel, G., Loveday, J. S., Weill, G. & Hull, S. (1992). *Physica B*, **180/181**, 907–910.

Bolzan, A. A., Fong, C., Kennedy, B. J. & Howard, C. J. (1993). *Aust. J. Chem.* **46**, 939–944.

Boman, C.-E. (1970). *Acta Chem. Scand.* **24**, 116–122.

Christy, A. G. (1993). *Acta Cryst.* B**49**, 987–996.

D'Antonio, P. & Santoro, A. (1980). *Acta Cryst.* B**36**, 2394–2397.

David, W. I. F., Akporiaye, D. E., Ibberson, R. M. & Wilson, C. C. (1988). Report RAL-103. Rutherford Appleton Laboratory, Didcot, England.

Gonzalez-Calbet, J. M. & Herrero, M. P. (1983). *Stud. Inorg. Chem.* **3**, 721–724.

Haines, J. & Léger, J. M. (1993). *Phys. Rev. B*, **48**, 13344–13350.

Haines, J. & Léger, J. M. (1997). *Phys. Rev. B*, **55**, 11144–11154.

Haines, J., Léger, J. M., Chateau, C., Pereira, A. S., Häusermann, D., Hanfland, M., Fiquet, G. & Andrault, D. (1997). Unpublished.

Haines, J., Léger, J. M. & Hoyau, S. (1995). *J. Phys. Chem. Solids*, **56**, 965–973.

Haines, J., Léger, J. M. & Schulte, O. (1996*a*). *J. Phys. Condens. Matter*, **8**, 1631–1646.

Haines, J., Léger, J. M. & Schulte, O. (1996*b*). *Science*, **271**, 629–631.

Hazen, R. M. & Finger, L. W. (1981). *J. Phys. Chem. Solids*, **42**, 143–151.

Hill, R. J. (1982). *Mater. Res. Bull.* **17**, 769–784.

Hill, R. J., Newton, M. D. & Gibbs, G. V. (1983). *J. Solid State Chem.* **47**, 185–200.

Hull, S., Smith, R. I., David, W. I. F., Hannon, A. C., Mayers, J. C. & Cywinski, R. (1992). *Physica B*, **180/181**, 1000–1002.

Hyde, B. G., Bursill, L. A., O'Keeffe, M. & Andersson, S. (1972). *Nature Phys. Sci.* **237**, 35–38.

Jauch, W., Palmer, A. & Schultz, A. J. (1993). *Acta Cryst.* B**49**, 984–987.

Jorgensen, J. D., Worlton, T. G. & Jamieson, J. C. (1978). *Phys. Rev. B*, **17**, 2212–2214.

Kingma, K. J., Cohen, R. E., Hemley, R. J. & Mao, H. K. (1995). *Nature*, **374**, 343–345.

Kudoh, Y. & Takeda, H. (1986). *Physica B*, **139/140**, 333–336.

Ross, N. L., Shu, J.-F., Hazen, R. M. & Gasparik, T. (1990). *Am. Mineral.* **75**, 739–747.

Tsuchida, Y. & Yagi, T. (1989). *Nature*, **340**, 217–220.

Wilson, R., Loveday, J. S., Nelmes, R. J., Klotz, S. & Marshall, W. G. (1995). *Nucl. Instrum. Methods A*, **354**, 145–148.